correlation is observed for the $L(O)Ni_2(pz)$ complex; i.e., this complex is more easily oxidized in stronger donor solvents whereas the ease of oxidation of $L(S)Ni_2(pz)$ is almost independent of the donor number.

(e) Controlled-Potential Electrolysis of $L(O)Ni_2(pz)$. As in the case of $L(S)Ni_2(pz)$ no evidence for stable $[L(O)Ni_2(pz)]^{2+}$, $[L(O)Ni_2(pz)]^{+}$, $[L(O)Ni_2(pz)]^{-}$, or $[L(O)Ni_2(pz)]^{2-}$ species could be obtained on the time scale of controlled-potential electrolysis. This is also consistent with other studies on related binuclear nickel complexes.[7a,c]

(f) Conclusions. The electrochemistry of $L(S)Ni_2(pz)$ and $L(O)Ni_2(pz)$ is characterized by two reduction processes

$$L(X)Ni_2(pz) + e^- \rightleftharpoons [L(X)Ni_2(pz)]^- \quad \text{(process I)} \quad (26)$$

$$[L(X)Ni_2(pz)]^- + e^- \rightleftharpoons [L(X)Ni_2(pz)]^{2-} \quad \text{(process II)} \quad (27)$$

which are separated by several hundred millivolts (X = S or O). This implies that strong interaction[30] is present for the mixed-valence species $[L(X)Ni_2(pz)]^-$. $L(S)Ni_2(pz)$ is not strongly solvated, and the separation in $(\Delta E_{1/2})_{I,II}^{red}$ is essentially solvent independent. In contrast, $L(O)Ni_2(pz)$ exists as a mixture of solvated species in coordinating solvents, which influences the redox chemistry. The reduced species $[L(X)Ni_2(pz)]^-$ and $[L(X)Ni_2(pz)]^{2-}$ are stabilized by nonspecific solvent effects present in polar solvents.

Oxidation of $L(X)Ni_2(pz)$ occurs via two barely resolved one-electron oxidation processes that are extremely solvent dependent:

$$L(X)Ni_2(pz) \rightleftharpoons [L(X)Ni_2(pz)]^+ + e^- \quad \text{(process III)} \quad (28)$$

$$[L(X)Ni_2(pz)]^+ \rightleftharpoons [L(X)Ni_2(pz)]^{2+} + e^- \quad \text{(process IV)} \quad (29)$$

That is, interactions in the mixed-valent complex $[L(X)Ni_2(pz)]^+$ are very weak[30] compared to the very strong interactions associated with the anionic binuclear complex $[L(X)Ni_2(pz)]^-$. A further two-electron process produces a highly reactive formally nickel(IV) species that is stabilized in coordinating solvents such as THF.

The remarkably different solvent effects associated with $L(S)Ni_2(pz)$ and $L(O)Ni_2(pz)$ are quite surprising because the distinction between the two complexes is only an endogenous bridging atom, O vs S. Interestingly, the sulfur binuclear complex is harder to oxidize than the oxygen one, contrary to normal expectations.[31] This implies that a structural difference influences the redox data in a manner that is not presently understood but illustrates the importance of the endogenous bridging center.

Acknowledgment. Work described in this paper was financially supported by the Australian Research Grants Scheme. The award of a Deakin University Gordon Research Fellowship and the assistance of the Japanese Ministry of Education enabling M.H. to spend a year's leave in Australia are also gratefully acknowledged.

Registry No. $L(S)Ni_2(pz)$, 111005-98-2; $[L(S)Ni_2(pz)]^-$, 111006-00-9; $[L(S)Ni_2(pz)]^{2-}$, 111006-01-0; $[L(S)Ni_2(pz)]^+$, 111006-02-1; $[L(S)Ni_2(pz)]^{2+}$, 111006-03-2; $L(O)Ni_2(pz)$, 111005-99-3; $[L(O)Ni_2(pz)]^-$, 111006-04-3; $[L(O)Ni_2(pz)]^{2-}$, 111006-05-4; $[L(O)Ni_2(pz)]^+$, 111006-06-5; $[L(O)Ni_2(pz)]^{2+}$, 111006-07-6; $L(O)Ni_2(pz)(DMF)_2$, 111006-08-7; DMF, 68-12-2; THF, 109-99-9; $L(S)H_2(C(O)NMe_2)$, 110480-99-4; $L(O)H_3$, 111006-09-8; C, 7440-44-0; Au, 7440-57-5; Pt, 7440-06-4; Hg, 7439-97-6; CH_2Cl_2, 75-09-2; PrCN, 109-74-0; acetone, 67-64-1; 2-amino-4,6-di-*tert*-butylphenol, 1643-39-6; 2-((*N*,*N*-dimethylcarbamoyl)thio)-5-methylisophthalaldehyde, 73729-07-4; 2-hydroxy-5-methylisophthalaldehyde, 7310-95-4.

(30) Robin, M. B.; Day, P. *Adv. Inorg. Chem. Radiochem.* **1967**, *10*, 247.

(31) Ray, D.; Pal, S.; Chakravorty, A. *Inorg. Chem.* **1986**, *25*, 2674.

Contribution from the Lehrstuhl für Anorganische Chemie I der Ruhr-Universität, D-4630 Bochum, FRG, Department of Chemistry and Laboratory for Molecular Structure and Bonding, Texas A&M University, College Station, Texas 77843, and Anorganisch-Chemisches Institut der Universität, D-6900 Heidelberg, FRG

Syntheses and Spectroscopic and Magnetic Properties of Novel Binuclear Vanadium(III/IV) Complexes. Crystal Structures of $[L_2V_2(\mu\text{-}O)(\mu\text{-}CH_3CO_2)_2]I_2\cdot 2H_2O$ and $[L_2V_2O_2(\mu\text{-}CH_3CO_2)_2]I_2$ (L = 1,4,7-Trimethyl-1,4,7-triazacyclononane)

Martin Köppen,[1a] Gerd Fresen,[1a] Karl Wieghardt,*[1a] Rosa M. Llusar,[1b] Bernhard Nuber,[1c] and Johannes Weiss[1c]

Received August 6, 1987

Hydrolysis of $[LVCl_3]\cdot$dmf (dmf = dimethylformamide) in aqueous sodium acetate solution under anaerobic conditions yields the green binuclear dication $[L_2V_2(\mu\text{-}O)(\mu\text{-}CH_3CO_2)_2]^{2+}$, which has been isolated as the diiodide dihydrate (L = 1,4,7-trimethyl-1,4,7-triazacyclononane, $C_9H_{21}N_3$). $[L_2V_2(\mu\text{-}O)(\mu\text{-}CH_3CO_2)_2]I_2\cdot 2H_2O$ crystallizes in the monoclinic system, space group $P2_1/c$, with $a = 8.836$ (5) Å, $b = 21.637$ (6) Å, $c = 18.560$ (7) Å, $\beta = 103.09$ (5)°, and $Z = 4$. The two vanadium(III) centers (d^2–d^2) are ferromagnetically spin exchange coupled ($H = -2J\hat{S}_1\hat{S}_2$; $S_1 = S_2 = 1$; $J = +22$ cm^{-1}; $g = 2.1$). Air oxidation of this green complex affords blue crystals of $[L_2V_2O_2(\mu\text{-}CH_3CO_2)_2]I_2$, which crystallizes in the orthorhombic space group $P2_12_12_1$ with $a = 21.665$ (2) Å, $b = 23.301$ (4) Å, $c = 13.161$ (2) Å, and $Z = 8$. It consists of binuclear bis(μ-acetato)-bis(vanadyl(IV)) dications. The terminal oxo groups are syn-positioned with respect to each other, and the nonbonded O···O distance is rather short (2.73 (1) Å), whereas the V···V distance is quite long (4.08 (1) Å). Strong intramolecular antiferromagnetic spin-exchange coupling between the two vanadyl ions (d^1–d^1) is observed ($J = -114$ cm^{-1}; $g = 2.2$). The green complex $[L'_2V_2(\mu\text{-}O)(\mu\text{-}CH_3CO_2)_2]$, where L′ represents the tridentate ligand hydrotripyrazolylborate(1−), has also been prepared; weak ferromagnetic exchange coupling ($J = +5$ cm^{-1}) is observed.

Introduction

Recently we have shown that binuclear metal centers bridged by an oxo group and two carboxylato groups, $[M_2(\mu\text{-}O)(\mu\text{-}CH_3CO_2)_2]$, form readily in aqueous ammonium acetate containing solutions using mononuclear complexes of the type LMX_3 as starting materials.[2a,3] L represents a suitable tridentate N-donor ligand, M has been iron(III)[2] or manganese(III),[3] respectively, and X^- is a unidentate ligand such as chloride or bromide. Studies using the saturated tridentate macrocycle 1,4,7-triazacyclononane[2] or its N-methylated derivative[2-4] and

(1) (a) Ruhr-Universität Bochum. (b) Texas A&M University. (c) Universität Heidelberg.

(2) (a) Wieghardt, K.; Pohl, K.; Gebert, W. *Angew. Chem., Int. Ed. Engl.* **1983**, *22*, 727. (b) Spool, A.; Williams, I. D.; Lippard, S. J. *Inorg. Chem.* **1985**, *24*, 2156.

(3) Wieghardt, K.; Bossek, U.; Ventur, D.; Weiss, J. *J. Chem. Soc., Chem. Commun.* **1985**, 347.

0020-1669/88/1327-0721$01.50/0

using the negatively charged tridentate ligand hydrotripyrazolylborate(1−)[5,6] have appeared. These low-molecular-weight binuclear complexes serve as structural models for the binding sites of two iron(III) centers in e.g. hemerythrin[12] or two manganese(III) ions in a recently characterized pseudocatalase from *Lactobacillus plantarum*.[7] In particular, the comparison of the magnetic properties of the model compounds with those of the biomolecules has proved to be very illuminating. We have now extended these studies to vanadium(III) complexes. We here wish to report the syntheses and spectroscopic and magnetic properties of $[L_2V_2(\mu\text{-}O)(\mu\text{-}CH_3CO_2)_2]I_2\cdot 2H_2O$ and of its oxidation product $[L_2V_2O_2(\mu\text{-}CH_3CO_2)_2]I_2$.

A preliminary report of this work has been communicated previously.[8]

Experimental Section

Preparation of Compounds. The ligands 1,4,7-trimethyl-1,4,7-triazacyclononane[9] and potassium hydrotripyrazolylborate[10] were prepared according to published procedures.

$[LVCl_3]$·dmf. To a clear solution of VCl_3 (1 g, 6.4 mmol) dissolved in dimethylformamide (dmf; 50 mL) under an argon atmosphere at 100 °C was added the ligand 1,4,7-trimethyl-1,4,7-triazacyclononane (L; 1.0 g, 0.64 mmol). An immediate color change to deep violet was observed. After this solution was refluxed for 1 h and cooled, a deep violet microcrystalline powder precipitated, which was filtered off, washed with ether, and dried under argon (yield 38%). The complex is insoluble in all common solvents and air-stable in the solid state. Anal. Calcd for $C_{12}H_{28}Cl_3N_4OV$: C, 35.88; H, 6.98; N, 13.95. Found: C, 35.85; H, 7.00; N, 13.90.

$[LVOCl_2]$. If the above reaction mixture was refluxed for 2 h in the presence of air, a deep green solution was obtained. From this solution blue crystals precipitated slowly within 2–3 weeks at room temperature (yield 22%). Anal. Calcd for $C_9H_{21}Cl_2N_3OV$: C, 34.95; H, 6.79; N, 13.59; Cl, 22.59. Found: C, 35.04; H, 6.73; N, 13.58; Cl 22.99.

$[L_2V_2(\mu\text{-}O)(\mu\text{-}CH_3CO_2)_2]I_2\cdot 2H_2O$. A suspension of sodium acetate (5 g) in H_2O (50 mL) and $[LVCl_3]$·dmf (1 g) was refluxed for 10 min under an argon atmosphere until a clear deep green solution was obtained, to which sodium iodide (5 g) was added. Within a few hours at room temperature deep green, needle-shaped crystals precipitated, which were filtered off, washed with ether, and air-dried (yield 20%). Anal. Calcd for $C_{22}H_{52}I_2N_6O_7V_2$: C, 30.42; H, 5.99; N, 9.68; I, 29.25. Found: C, 30.38; H, 5.89; N, 9.89; I, 29.48.

$[L'_2V_2(\mu\text{-}O)(\mu\text{-}CH_3CO_2)_2]$. To a red solution of VCl_3 (1 g) in dmf (50 mL) under an argon atmosphere was added potassium hydrotripyrazolylborate (L'). Refluxing for 2 h yielded a clear violet solution, from which the solvent was removed under reduced pressure. The resulting violet material was dissolved in degassed 0.5 M aqueous sodium acetate (50 mL). From this solution a green precipitate was obtained within a few minutes, which was filtered off and recrystallized from acetonitrile (yield 46%). Anal. Calcd for $C_{22}H_{26}B_2N_{12}O_5V_2$: C, 39.91; H, 3.96; N, 25.38. Found: C, 39.66; H, 3.99; N, 25.33.

$[L_2V_2O_2(\mu\text{-}CH_3CO_2)_2]I_2$. Method A. When the deep green filtrate of the solution obtained from the preparation of $[L_2V_2(\mu\text{-}O)(\mu\text{-}CH_3CO_2)_2]I_2\cdot 2H_2O$ was allowed to stand in an open vessel in the presence of air, two different types of crystals precipitated, which were readily separated manually under a microscope. Blue crystals of $[L_2V_2O_2(\mu\text{-}CH_3CO_2)_2]I$ were obtained, as well as violet crystals, which differed in composition from sample to sample and were discarded. The yield of the blue crystals was low (~5% related to starting $[LVCl_3]$·dmf).

Method B. Blue $[LVOCl_2]$ (0.5 g, 1.6 mmol) was dissolved at 60 °C in an aqueous solution (50 mL) that contained sodium acetate (2 g). After 30 min the blue solution was cooled to 15 °C and sodium iodide (2 g) was added with stirring. Within 2 days at 10 °C blue crystals of $[L_2V_2O_2(\mu\text{-}CH_3CO_2)_2]I_2$ precipitated, which were filtered off, washed with ethanol and ether, and air-dried (yield 35%). Anal. Calcd for $C_{22}H_{48}I_2N_6O_6V_2$: C, 31.13; H, 5.66; N, 9.90; I, 29.95. Found: C, 31.19; H, 5.67; N, 9.51; I, 29.90.

Table I. Data for Crystal-Structure Analysis

compd	$[L_2V_2(\mu\text{-}O)(\mu\text{-}CH_3CO_2)_2I_2\cdot 2H_2O$	$[L_2V_2O_2(\mu\text{-}CH_3CO_2)_2]I_2$
formula	$C_{22}H_{52}N_6O_7I_2V_2$	$C_{22}H_{48}N_6O_6I_2V_2$
M_r	868.4	848.36
cryst syst	monoclinic	orthorhombic
space group	$P2_1/c$	$P2_12_12_1$
a, Å	8.836 (7)	21.665 (2)
b, Å	21.637 (4)	23.301 (4)
c, Å	18.560 (9)	13.161 (2)
β, deg	103.09 (5)	90.0
V, Å^3	3456.3 (10)	6644 (2)
Z	4	8
D_{calcd}, g cm^{-3}	1.67	1.7
instrument	AED II (Siemens)	Enraf-Nonius CAD 4
μ(Mo Kα), cm^{-1}	22.1	24.25
radiation	Mo Kα, graphite monochromatized (λ = 0.71073 Å)	
cryst size, mm^3	0.25 × 0.27 × 0.54	0.3 × 0.4 × 0.4
transmission coeff (min, max)	0.468, 0.578	0.967, 0.995
T, K	293	288
scan method	ω	ω–2θ
2θ range, deg	$3 \leq 2\theta \leq 60$	$4 \leq 2\theta \leq 45$
no. of rflns measd	4262 ($\pm h,k,l$)	4469
no. of obsd data	4190 ($I \geq 1.5\sigma(I)$)	3992 ($I \geq 3\sigma(I)$)
no. of params refined	342	685
R[a]	0.049	0.048
R_w[b]	0.038	0.061
GOF[c]	1.8	1.88
shift/esd in last cycle		
mean	0.01	0.005
max	0.24	0.01

[a] $R = \sum||F_o| - |F_c||/\sum|F_o|$. [b] $R_w = [\sum w(|F_o| - |F_c|)^2/\sum w|F_o|^2]^{1/2}$; $w = 1/\sigma^2(F)$. [c] Quality of $[\sum w(|F_o| - |F_c|)^2/(N_{observns} - N_{params})]^{1/2}$.

Physical Measurements. Electronic spectra were recorded on a Perkin-Elmer Lambda 9 spectrophotometer; infrared spectra were obtained on KBr disks with a Beckman Acculab 10 spectrophotometer. Magnetic susceptibilities of powdered samples were measured by the Faraday method (Sartorius microbalance and Bruker B-E10 C8 research magnet and B-VT 1000 automatic temperature control) in the temperature range 100–293 K. Diamagnetic corrections were applied in the usual manner with use of Pascal's constants. Electrochemical measurements were performed with a Princeton Applied Research Model 175 programmer, 173 potentiostat and 179 digital coulometer and a Kipp & Zonen XY recorder on acetonitrile solutions that were 0.1 M in $[n\text{-}Bu_4N]PF_6$. A standard three-electrode cell was employed with a glassy-carbon working electrode, a Pt-wire auxiliary electrode, and an Ag/AgCl reference electrode (saturated LiCl/ethanol). Potentials are referenced versus the ferrocenium/ferrocene couple as internal standard. Cyclic voltammograms were recorded at scan rates from 20 to 500 mV s^{-1}; the concentration of the electroactive component was ~5 × 10^{-4} M.

X-ray Crystallography. The crystals selected, green $[L_2V_2(\mu\text{-}O)(\mu\text{-}CH_3CO_2)_2]I_2\cdot 2H_2O$ (**1**) and blue $[L_2V_2O_2(\mu\text{-}CH_3CO_2)_2]I_2$ (**2**), were mounted in glass capillaries and sealed under nitrogen. The cell constants of **1** and **2** were obtained from a least-squares fit of 25 reflections in the range $17 < 2\theta < 28°$ and confirmed by axial photographs. Data were collected on a single-crystal four-circle diffractometer using graphite-monochromated Mo Kα radiation. Crystal data and details of the parameters associated with data collection are given in Table I. Data were corrected for Lorentz and polarization effects as well as absorption. The absorption corrections for **1** and **2** were based on an empirical method that uses ψ scans of nine reflections with diffractometer angle χ near 90°.

The structure of **1** was solved via conventional Patterson and Fourier syntheses. The structure was refined by use of block-cascade least-squares methods with anisotropic temperature factors for all non-hydrogen atoms. The quantity minimized was $\sum w(|F_o| - |F_c|)^2$, where the weights w were taken as $1/\sigma^2(I)$. The contribution of hydrogen atoms bound to carbon was introduced in calculated positions (C–H = 0.96 Å and sp^3-hybridized carbon atoms). These hydrogen atoms were assumed to have isotropic thermal motion. The STRUCSY suite of crystallographic

(4) Chaudhuri, P.; Wieghardt, K.; Nuber, B.; Weiss, J. *Angew. Chem., Int. Ed. Engl.* **1985**, *24*, 778.
(5) (a) Armstrong, W. H.; Lippard, S. J. *J. Am. Chem. Soc.* **1983**, *105*, 4837. (b) Armstrong, W. H.; Spool, A.; Papaefthymiou, G. C.; Frankel, R. B.; Lippard, S. J. *J. Am. Chem. Soc.* **1984**, *106*, 3653.
(6) Sheats, J. E.; Czernuszewicz, R. S.; Dismukes, G. C.; Rheingold, A. L.; Petrouleas, V.; Stubbe, J.; Armstrong, W. H.; Beer, R. H.; Lippard, S. J. *J. Am. Chem. Soc.* **1987**, *109*, 1435.
(7) Beyer, W. F.; Fridovich, I. *Biochemistry* **1985**, *24*, 6460.
(8) Wieghardt, K.; Köppen, M.; Nuber, B.; Weiss, J. *J. Chem. Soc., Chem. Commun.* **1986**, *1530*.
(9) Wieghardt, K.; Chaudhuri, P.; Nuber, B.; Weiss, J. *Inorg. Chem.* **1982**, *21*, 3086.
(10) Trofimenko, S. *J. Am. Chem. Soc.* **1967**, *79*, 3170.
(11) *International Tables for X-ray Crystallography*; Kynoch: Birmingham, England, 1974; Vol. IV, pp 99, 149.
(12) Stenkamp, R. E.; Sieker, L. C.; Jensen, L. H.; Sanders-Loehr, J. *Nature (London)* **1981**, *291*, 263.

Table II. Positions of Non-Hydrogen Atoms ($\times 10^4$) with Estimated Standard Deviations (Esd) in Parentheses for $[L_2V_2(\mu\text{-}O)(\mu\text{-}CH_3CO_2)_2]I_2\cdot 2H_2O$

atom	x	y	z
V(1)	5662 (1)	796.6 (5)	2196.6 (6)
V(2)	3518 (1)	1692.1 (5)	971.8 (6)
O(1)	4790 (4)	1516 (2)	1843 (2)
O(2)	6573 (5)	690 (2)	1288 (2)
O(3)	4666 (4)	1099 (2)	416 (2)
O(4)	3719 (5)	310 (2)	1717 (2)
O(5)	2008 (5)	997 (2)	1103 (3)
C(1)	2365 (8)	473 (4)	1379 (4)
C(2)	1110 (8)	5012 (3)	6280 (4)
C(3)	5914 (8)	802 (3)	615 (4)
C(4)	6671 (8)	570 (3)	44 (4)
C(11)	2825 (8)	3023 (3)	1249 (4)
C(12)	4499 (8)	2961 (3)	1207 (4)
C(13)	3925 (8)	2693 (3)	−125 (4)
C(14)	2949 (8)	2817 (3)	4452 (4)
C(15)	687 (8)	2657 (4)	4987 (4)
C(16)	556 (7)	2649 (3)	5790 (4)
C(17)	1934 (8)	2294 (3)	2068 (4)
C(18)	6348 (7)	2614 (3)	5708 (4)
C(19)	1208 (8)	3654 (3)	4484 (4)
C(21)	5514 (8)	147 (3)	3642 (4)
C(22)	5688 (8)	−340 (3)	3088 (4)
C(23)	8313 (8)	5033 (3)	8010 (4)
C(24)	8945 (8)	4412 (4)	7831 (4)
C(25)	7724 (7)	3982 (3)	8650 (4)
C(26)	6026 (8)	3724 (3)	8671 (4)
C(27)	3415 (7)	4110 (3)	8238 (4)
C(28)	6645 (9)	5571 (3)	6984 (4)
C(29)	8427 (8)	3333 (3)	7558 (4)
I(1)	8105.5 (6)	4257.7 (3)	701.8 (3)
I(2)	6529.9 (6)	3088.3 (2)	3466.9 (3)
$O_w(1)$	1527 (6)	850 (3)	4922 (3)
$O_w(2)$	9411 (8)	3474 (4)	2433 (4)
N(1)	2103 (6)	2399 (2)	1303 (3)
N(2)	4677 (5)	2488 (2)	651 (3)
N(3)	1932 (6)	1896 (3)	−125 (3)
N(4)	5085 (6)	761 (3)	3269 (3)
N(5)	6692 (6)	−113 (2)	2587 (3)
N(6)	7869 (6)	1100 (2)	2858 (3)

programs (Stoe, Darmstadt, FRG) was used for all calculations. Atomic scattering factors, including anomalous dispersion, were taken from ref 11. Final positional parameters for **1** are given in Table II, and selected bond lengths and angles appear in Table III.

The structure of **2** was solved with the positions of the iodine atoms determined by direct methods. The other atoms were then found in a series of alternating refinements and difference maps. The structure of **2** was refined with anisotropic thermal parameters for all non-hydrogen atoms. No attempt was made to locate the hydrogen atoms, and they were not included in calculated positions in the final refinement. Residuals for the final refinement cycle are given in Table I; those for the alternative enantiomorph were $R = 0.051$ and $R_w = 0.067$. Positional parameters for **2** are given in Table IV; selected bond lengths and angles are summarized in Tables V and VI, respectively.

Results and Discussion

Synthesis. A simple synthetic route to compounds containing the (μ-oxo)bis(μ-acetato)dimetal(III) core is the reaction of mononuclear complexes of the type $LMCl_3$ (L represents the tridentate ligands 1,4,7-triazacyclononane, 1,4,7-trimethyl-1,4,7-triazacyclononane, and hydrotripyrazolylborate(1−)) with sodium acetate in aqueous solution.[2a,3,4] This approach has now

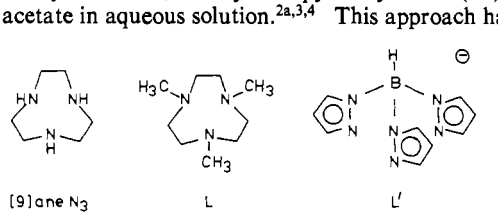

been successfully extended to vanadium(III). Thus, VCl_3 dissolved in dry dimethylformamide (dmf) reacts at elevated temperatures with tridentate N-donors to yield violet microcrystalline $[LVCl_3]\cdot$dmf or $K[L'VCl_3]$. The latter has not been further

Table III. Selected Bond Distances (Å) and Angles (deg) of $[L_2V_2(\mu\text{-}O)(\mu\text{-}CH_3CO_2)_2]I_2\cdot 2H_2O$

V(1)–O(1)	1.794 (4)	V(2)–O(1)	1.789 (4)
V(1)–O(2)	2.039 (4)	V(2)–O(3)	2.052 (4)
V(1)–O(4)	2.039 (5)	V(2)–O(5)	2.062 (4)
V(1)–N(4)	2.166 (5)	V(2)–N(1)	2.152 (5)
V(1)–N(5)	2.219 (5)	V(2)–N(2)	2.155 (5)
V(1)–N(6)	2.158 (5)	V(2)–N(3)	2.238 (5)
O(2)–C(3)	1.276 (8)	O(4)–C(1)	1.269 (9)
O(3)–C(3)	1.258 (8)	O(5)–C(1)	1.254 (10)
C(1)–C(2)	1.507 (10)	C(3)–C(4)	1.46 (1)
V(1)···V(2)	3.250 (2)		
O(1)–V(1)–O(2)	90.8 (2)	O(1)–V(1)–N(4)	101.3 (3)
O(1)–V(1)–N(6)	101.6 (3)	O(2)–V(1)–N(4)	167.3 (2)
O(2)–V(1)–N(6)	91.7 (3)	O(4)–V(1)–N(5)	85.0 (3)
N(4)–V(1)–N(5)	80.4 (3)	N(5)–V(1)–N(6)	80.4 (3)
O(1)–V(1)–O(4)	92.2 (2)	O(1)–V(1)–N(5)	177.8 (5)
O(2)–V(1)–O(4)	91.8 (3)	O(2)–V(1)–N(5)	87.7 (3)
O(4)–V(1)–N(4)	91.9 (3)	O(4)–V(1)–N(6)	165.6 (2)
N(4)–V(1)–N(6)	81.8 (3)		
O(1)–V(2)–O(3)	92.4 (2)	O(1)–V(2)–N(1)	100.4 (3)
O(1)–V(2)–N(3)	180.0 (6)	O(3)–V(2)–N(1)	166.9 (2)
O(3)–V(2)–N(3)	86.8 (2)	O(5)–V(2)–N(2)	167.7 (2)
N(1)–V(2)–N(2)	81.6 (2)	N(2)–V(2)–N(3)	80.3 (2)
O(1)–V(2)–O(5)	91.6 (2)	O(1)–V(2)–N(2)	100.4 (3)
O(3)–V(2)–O(5)	90.6 (2)	O(3)–V(2)–N(2)	92.4 (3)
O(5)–V(2)–N(1)	93.0 (3)	O(5)–V(2)–N(3)	87.8 (3)
N(1)–V(2)–N(3)	80.5 (3)		
V(1)–O(1)–V(2)	130.2 (2)		
V(1)–O(2)–C(3)	127.6 (5)	V(2)–O(3)–C(3)	132.3 (6)
V(1)–O(4)–C(1)	132.7 (7)	V(2)–O(5)–C(1)	126.7 (6)
O(2)–C(3)–O(3)	124.1 (5)	O(2)–C(3)–C(4)	117.5 (6)
O(4)–C(1)–O(5)	125.2 (6)	O(3)–C(3)–C(4)	118.4 (6)
O(4)–C(1)–C(2)	116.9 (7)	O(5)–C(1)–C(2)	118.0 (7)

characterized. From temperature-dependent (100–300 K) magnetic susceptibility measurements on $[LVCl_3]\cdot$dmf a temperature-independent magnetic moment of 2.90 μ_B was deduced, which is characteristic for mononuclear octahedral vanadium(III) (the spin-only value for d^2 is 2.83 μ_B). Hydrolyses of these mononuclear species in an aqueous solution of sodium acetate at 100 °C under anaerobic conditions gave deep green solutions from which green microcrystals of $[L'_2V_2(\mu\text{-}O)(\mu\text{-}CH_3CO_2)_2]$ precipitated if the ligand was hydrotripyrazolylborate, whereas in the case of the neutral ligand 1,4,7-trimethyl-1,4,7-triazacyclononane the addition of sodium iodide to the green reaction mixture afforded green crystals of $[L_2V_2(\mu\text{-}O)(\mu\text{-}CH_3CO_2)_2]I_2\cdot 2H_2O$.

In the infrared spectrum of the former material two bands at 1540 and 1440 cm^{-1} are indicative of the symmetrical acetate bridges (ν_{as}(CO) and ν_s(CO)), and a band at 660 cm^{-1} is assigned to the antisymmetrical V–O stretching mode of a (V–O–V) moiety. For $[L_2V_2(\mu\text{-}O)(\mu\text{-}CH_3CO_2)_2]I_2\cdot 2H_2O$ the ν_{as}(CO) and ν_s(CO) bands of the acetato bridges are observed at 1560 cm^{-1} and 1468, 1430 cm^{-1}; ν_{as}(V–O–V) is at 670 cm^{-1}.

While the vanadium(III) dimers are stable toward air in the solid state, in solution they react with oxygen to produce oxovanadium(IV) species. Thus, exposure to air of the filtrate of the reaction mixture that produced $[L_2V_2(\mu\text{-}O)(\mu\text{-}CH_3CO_2)_2]I_2\cdot 2H_2O$ afforded upon slow evaporation of the solvent water within a few weeks a mixture of solid sodium acetate and sodium iodide (both colorless) as well as well-grown blue crystals and a violet crystalline material. These were manually segregated. The exact nature of the violet crystals was not established since their analytical composition varied strongly in three different preparations. In contrast, the blue crystals were of the same homogeneous composition, which an X-ray single-crystal structure analysis (see below) showed to be the dimer $[L_2V_2O_2(\mu\text{-}CH_3CO_2)_2]I_2$.

A more rational synthesis of this material was subsequently found. Hydrolysis of monomeric $LVOCl_2$ in an aqueous solution of sodium acetate gave after addition of sodium iodide blue crystals of $[L_2V_2O_2(\mu\text{-}CH_3CO_2)_2]I_2$. Bands in the infrared spectrum at 1570 cm^{-1} (ν_{as} (CO)) and 1450, 1410 cm^{-1} (ν_s(CO)) are again indicative of symmetrical μ-acetato bridges. The blue monomeric

Table IV. Atomic Positional Parameters and Equivalent Isotropic Displacement Parameters (Å^2) and Their Estimated Standard Deviations for $[V_2O_2(CH_3COO)_2L_2]I_2$[a]

atom	x	y	z	B	atom	x	y	z	B
V(1)	0.2661 (1)	0.27359 (8)	0.5111 (2)	2.95 (4)	O(2)	0.4186 (4)	0.4582 (4)	0.6143 (6)	3.9 (2)
V(3)	0.2659 (1)	0.20030 (8)	0.2300 (1)	2.67 (4)	O(4)	0.4105 (4)	0.4115 (4)	0.4184 (7)	5.2 (2)
O(1)	0.3098 (5)	0.3037 (4)	0.4314 (7)	5.4 (2)	O(21)	0.4506 (4)	0.5616 (4)	0.5143 (6)	3.8 (2)
O(3)	0.3038 (4)	0.2574 (4)	0.2412 (7)	4.0 (2)	O(22)	0.5444 (4)	0.4804 (4)	0.5699 (6)	3.9 (2)
O(11)	0.1848 (4)	0.2629 (4)	0.4396 (6)	4.0 (2)	O(41)	0.4468 (4)	0.5236 (4)	0.3583 (6)	4.2 (2)
O(12)	0.2876 (4)	0.1902 (4)	0.5006 (7)	4.6 (2)	O(42)	0.5381 (4)	0.4386 (4)	0.4176 (6)	3.9 (2)
O(31)	0.1841 (4)	0.2169 (4)	0.2910 (6)	3.9 (2)	N(21)	0.4009 (4)	0.5596 (4)	0.7186 (7)	3.2 (2)
O(32)	0.2917 (4)	0.1510 (4)	0.3458 (6)	3.9 (2)	N(22)	0.5277 (5)	0.5809 (4)	0.6955 (7)	3.4 (2)
N(11)	0.2349 (5)	0.3556 (4)	0.5720 (8)	4.0 (2)	N(23)	0.4893 (4)	0.4772 (4)	0.7784 (7)	3.0 (2)
N(12)	0.3332 (5)	0.2814 (5)	0.6323 (8)	3.7 (2)	N(41)	0.5189 (5)	0.4626 (5)	0.2032 (7)	3.9 (2)
N(13)	0.2100 (5)	0.2467 (5)	0.6550 (8)	3.6 (2)	N(42)	0.4786 (5)	0.3552 (4)	0.2759 (8)	4.0 (2)
N(31)	0.2340 (5)	0.2273 (4)	0.0837 (7)	3.5 (2)	N(43)	0.3907 (5)	0.4405 (5)	0.2196 (8)	4.2 (2)
N(32)	0.3369 (4)	0.1586 (4)	0.1382 (8)	3.5 (2)	C(5)	0.4428 (5)	0.5644 (5)	0.4201 (9)	3.2 (3)
N(33)	0.2153 (5)	0.1190 (4)	0.1677 (7)	3.1 (2)	C(6)	0.4241 (7)	0.6236 (5)	0.373 (1)	4.6 (3)
C(1)	0.1584 (5)	0.2382 (5)	0.3682 (9)	2.9 (3)	C(7)	0.5666 (6)	0.4565 (5)	0.4948 (9)	3.2 (3)
C(2)	0.0882 (6)	0.2345 (6)	0.372 (1)	4.6 (3)	C(8)	0.6367 (6)	0.4468 (6)	0.495 (1)	4.0 (3)
C(3)	0.2973 (5)	0.1492 (5)	0.441 (1)	3.4 (3)	C(21)	0.4228 (7)	0.6206 (5)	0.718 (1)	4.2 (3)
C(4)	0.3177 (7)	0.0946 (5)	0.489 (1)	4.8 (3)	C(22)	0.4893 (6)	0.6248 (5)	0.750 (1	3.8 (3)
C(11)	0.2937 (6)	0.3828 (6)	0.608 (1)	4.4 (3)	C(23)	0.5691 (6)	0.5514 (5)	0.764 (1)	3.7 (3)
C(12)	0.3306 (7)	0.3424 (6)	0.675 (1)	5.6 (4)	C(24)	0.5342 (6)	0.5130 (6)	0.833 (1)	3.9 (3)
C(13)	0.3169 (7)	0.2392 (6)	0.717 (1)	5.1 (4)	C(25)	0.4284 (6)	0.4770 (6)	0.833 (1)	3.9 (3)
C(14)	0.2502 (6)	0.2423 (5)	0.743 (1)	4.1 (3)	C(26)	0.3985 (6)	0.5369 (6)	0.826 (1)	4.2 (3)
C(15)	0.1616 (6)	0.2925 (6)	0.665 (1)	4.2 (3)	C(27)	0.3362 (6)	0.5561 (7)	0.671 (1)	4.9 (3)
C(16)	0.1907 (6)	0.3520 (6)	0.658 (1)	4.1 (3)	C(28)	0.5675 (6)	0.6091 (6)	0.614 (1)	4.4 (3)
C(17)	0.2037 (8)	0.3917 (6)	0.493 (1)	6.0 (4)	C(29)	0.5108 (6)	0.4160 (5)	0.771 (1)	4.0 (3)
C(18)	0.3962 (6)	0.2683 (9)	0.601 (1)	7.4 (5)	C(41)	0.5538 (9)	0.4107 (7)	0.185 (2)	12.9 (5)
C(19)	0.1776 (8)	0.1890 (6)	0.643 (1)	5.4 (4)	C(42)	0.5290 (7)	0.3580 (7)	0.205 (1)	5.7 (4)
C(31)	0.2935 (7)	0.2345 (6)	0.028 (1)	4.6 (3)	C(43)	0.4178 (8)	0.3390 (6)	0.224 (2)	7.3 (5)
C(32)	0.3323 (7)	0.1837 (6)	0.032 (1)	4.7 (3)	C(44)	0.3791 (9)	0.3761 (7)	0.194 (2)	9.2 (5)
C(33)	0.3244 (6)	0.0962 (5)	0.141 (1)	3.6 (3)	C(45)	0.4124 (7)	0.4737 (8)	0.134 (1)	7.3 (4)
C(34)	0.2593 (6)	0.0823 (5)	0.112 (1)	3.9 (3)	C(46)	0.4754 (9)	0.481 (1)	0.124 (1)	12.8 (5)
C(35)	0.1672 (6)	0.1432 (6)	0.100 (1)	4.4 (3)	C(47)	0.5617 (6)	0.5111 (6)	0.224 (1)	4.7 (3)
C(36)	0.1935 (6)	0.1853 (6)	0.029 (1)	4.1 (3)	C(48)	0.493 (1)	0.3143 (6)	0.357 (1)	8.6 (6)
C(37)	0.2009 (7)	0.2839 (5)	0.091 (1)	5.0 (3)	C(49)	0.3307 (7)	0.4702 (8)	0.251 (1)	6.9 (5)
C(38)	0.3985 (6)	0.1694 (6)	0.181 (1)	4.5 (3)	I(1)	−0.00648 (4)	0.85639 (4)	0.94924 (7)	4.65 (2)
C(39)	0.1858 (7)	0.0846 (6)	0.251 (1)	4.7 (3)	I(2)	0.25431 (5)	0.93339 (4)	0.31011 (7)	4.89 (2)
V(2)	0.46494 (9)	0.50912 (8)	0.6294 (1)	2.55 (4)	I(3)	0.73272 (5)	0.92189 (5)	0.57491 (7)	5.01 (2)
V(4)	0.45697 (9)	0.43918 (9)	0.3429 (2)	2.90 (4)	I(4)	−0.00576 (7)	0.73101 (5)	0.4427 (1)	9.07 (4)

[a] Anisotropically refined atoms are given in the form of the equivalent isotropic displacement parameter defined as $^4/_3[a^2\beta_{11} + b^2\beta_{22} + c^2\beta_{33} + ab(\cos\gamma)\beta_{12} + ac(\cos\beta)\beta_{13} + bc(\cos\alpha)\beta_{23}]$.

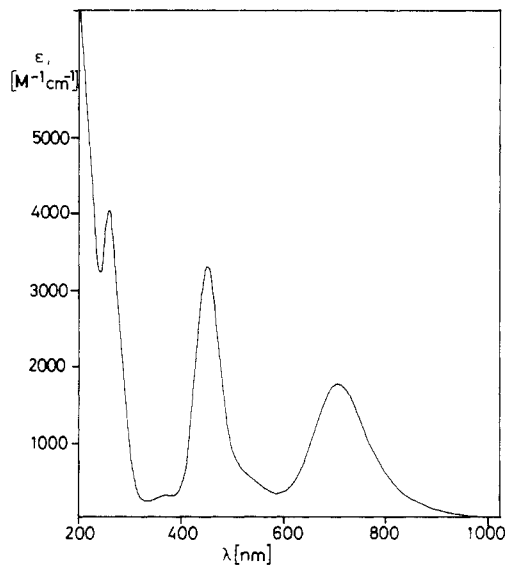

Figure 1. Electronic spectrum of $[L_2V_2(\mu\text{-}O)(\mu\text{-}CH_3CO_2)_2]I_2\cdot 2H_2O$ in acetonitrile.

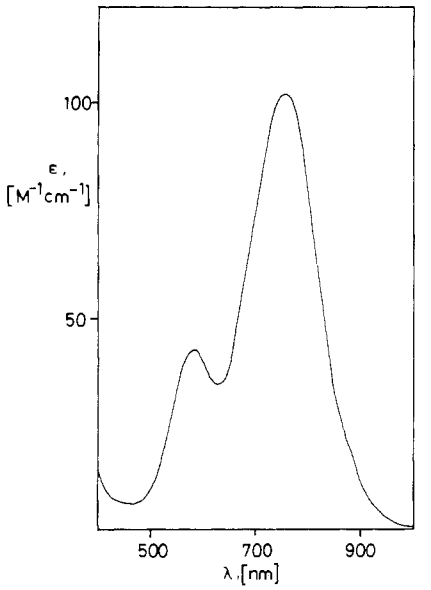

Figure 2. Electronic spectrum of $[L_2V_2O_2(\mu\text{-}CH_3CO_2)_2]I_2$ in acetonitrile.

$LVOCl_2$ was obtained from $[LVCl_3]$·dmf via air oxidation in dmf. It is a monomeric vanadyl complex (μ = 1.79 μ_B (100–298 K), ν(V=O) = 940 cm^{-1}).

Electronic Spectra. Table VII summarizes the electronic spectra and magnetic properties of the new complexes. Figures 1 and2 show the solution UV–vis spectra of $[L_2V_2(\mu\text{-}O)(\mu\text{-}CH_3CO_2)_2]I_2\cdot 2H_2O$ and $[L_2V_2O_2(\mu\text{-}CH_3CO_2)_2]I_2$ in acetonitrile, respectively. The spectrum of $[L_2V_2(\mu\text{-}O)(\mu\text{-}CH_3CO_2)_2]^{2+}$ is very unusual. It exhibits three very strong absorption bands with molar extinction coefficients >10^3 M^{-1} cm^{-1}, two of which absorb in the visible region and one of which is in the ultraviolet region. The spectrum of $[L'_2V_2(\mu\text{-}O)(\mu\text{-}CH_3CO_2)_2]$ is very similar, although

Table V. Bond Distances (Å) and Their Estimated Standard Deviations for $[V_2O_2(CH_3COO)_2L_2]I_2$[a]

V(1)–O(1)	1.578 (10)	V(3)–O(32)	1.988 (8)	V(2)–N(22)	2.323 (10)
V(1)–O(11)	2.013 (8)	V(3)–N(31)	2.141 (10)	V(2)–N(23)	2.163 (9)
V(1)–O(12)	2.003 (9)	V(3)–N(32)	2.185 (10)	V(4)–O(4)	1.554 (10)
V(1)–N(11)	2.181 (10)	V(3)–N(33)	2.337 (10)	V(4)–O(41)	1.990 (9)
V(1)–N(12)	2.165 (10)	V(2)–O(2)	1.565 (9)	V(4)–O(42)	2.014 (8)
V(1)–N(13)	2.336 (10)	V(2)–O(21)	1.972 (8)	V(4)–N(41)	2.341 (10)
V(3)–O(3)	1.570 (9)	V(2)–O(22)	2.007 (8)	V(4)–N(42)	2.197 (10)
V(3)–O(31)	1.983 (8)	V(2)–N(21)	2.164 (10)	V(4)–N(43)	2.167 (11)

[a] Numbers in parentheses are estimated standard deviations in the least significant digits.

Table VI. Bond Angles (deg) and Their Estimated Standard Deviations for $[V_2O_2(CH_3COO)_2L_2]I_2$[a]

O(1)–V(1)–O(11)	105.6 (4)	O(31)–V(3)–O(32)	93.1 (4)	O(22)–V(2)–N(22)	83.3 (4)
O(1)–V(1)–O(12)	104.3 (5)	O(31)–V(3)–N(31)	91.1 (4)	O(22)–V(2)–N(23)	91.7 (3)
O(1)–V(1)–N(11)	92.3 (5)	O(31)–V(3)–N(32)	160.0 (4)	N(21)–V(2)–N(22)	77.4 (4)
O(1)–V(1)–N(12)	92.9 (5)	O(31)–V(3)–N(33)	83.2 (4)	N(21)–V(2)–N(23)	81.5 (4)
O(1)–V(1)–N(13)	166.1 (4)	O(32)–V(3)–N(31)	161.8 (4)	N(22)–V(2)–N(23)	76.4 (4)
O(11)–V(1)–O(12)	92.9 (4)	O(32)–V(3)–N(32)	88.2 (4)	O(4)–V(4)–O(41)	105.8 (5)
O(11)–V(1)–N(11)	90.5 (4)	O(32)–V(3)–N(33)	86.1 (3)	O(4)–V(4)–O(42)	104.5 (4)
O(11)–V(1)–N(12)	160.4 (4)	N(31)–V(3)–N(32)	81.9 (4)	O(4)–V(4)–N(41)	166.0 (5)
O(11)–V(1)–N(13)	83.7 (3)	N(31)–V(3)–N(33)	76.8 (4)	O(4)–V(4)–N(42)	91.5 (5)
O(12)–V(1)–N(11)	161.4 (4)	N(32)–V(3)–N(33)	77.0 (4)	O(4)–V(4)–N(43)	93.2 (5)
O(12)–V(1)–N(12)	88.7 (4)	O(2)–V(2)–O(21)	105.7 (4)	O(41)–V(4)–O(42)	93.1 (4)
O(12)–V(1)–N(13)	85.2 (4)	O(2)–V(2)–O(22)	104.4 (4)	O(41)–V(4)–N(41)	85.0 (4)
N(11)–V(1)–N(12)	82.1 (4)	O(2)–V(2)–N(21)	94.0 (4)	O(41)–V(4)–N(42)	160.9 (4)
N(11)–V(1)–N(13)	77.0 (4)	O(2)–V(2)–N(22)	165.3 (4)	O(41)–V(4)–N(43)	89.4 (4)
N(12)–V(1)–N(13)	77.0 (4)	O(2)–V(2)–N(23)	90.6 (4)	O(42)–V(4)–N(41)	83.4 (3)
O(3)–V(3)–O(31)	105.3 (4)	O(21)–V(2)–O(22)	92.4 (3)	O(42)–V(4)–N(42)	90.2 (4)
O(3)–V(3)–O(32)	105.7 (4)	O(21)–V(2)–N(21)	88.8 (4)	O(42)–V(4)–N(43)	160.7 (4)
O(3)–V(3)–N(31)	90.2 (4)	O(21)–V(2)–N(22)	86.2 (3)	N(41)–V(4)–N(42)	76.7 (4)
O(3)–V(3)–N(32)	93.5 (4)	O(21)–V(2)–N(23)	161.6 (4)	N(41)–V(4)–N(43)	77.8 (4)
O(3)–V(3)–N(33)	164.8 (4)	O(22)–V(2)–N(21)	160.5 (4)	N(42)–V(4)–N(43)	81.5 (4)

[a] Numbers in parentheses are estimated standard deviations in the least significant digits.

Table VII. Electronic Spectra and Magnetic Properties of Complexes

complex	color	λ_{max}, nm (ϵ, M^{-1} cm^{-1})[a]	μ_{eff}(293 K), μ_B	J, cm^{-1}
$[LVCl_3]$·dmf	violet	497, 700 sh[b]	2.90	
$[LVOCl_2]$	blue	667 (23.5), 760 sh (14)	1.79	
$[L_2V_2(\mu\text{-O})(\mu\text{-}CH_3CO_2)_2]I_2\cdot 2H_2O$	green	258 (4.1 × 10^3), 449 (3.6 × 10^3), 709 (1.9 × 10^3)	3.25 (293 K), 3.40 (103 K)[c]	+22
$[L'_2V_2(\mu\text{-O})(\mu\text{-}CH_3CO_2)_2]$	green	439 (2.2 × 10^3), 673 (1.7 × 10^3)	3.18 (293 K), 3.33 (103 K)[c]	+5
$[L_2V_2O_2(\mu\text{-}CH_3CO_2)_2]I_2$	blue	583 (42), 755 (101)	1.60 (293 K), 0.85 (113 K)[c]	−114

[a] Measured in acetonitrile; where appropriate, ϵ values are per dimer. [b] Reflectance spectrum. [c] μ_{eff} per vanadium center.

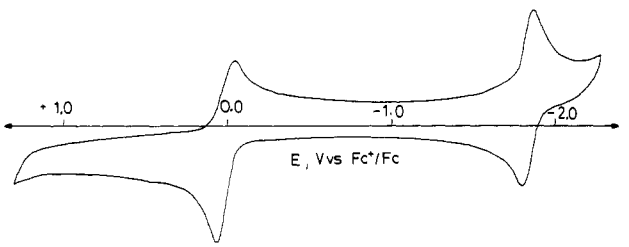

Figure 3. Cyclic voltammogram of $[L_2V_2(\mu\text{-O})(\mu\text{-}CH_3CO_2)_2](PF_6)_2$ in 0.1 M $[TBA]PF_6$/acetonitrile (glassy-carbon electrode; scan rate 50 mV s^{-1}; 25 °C).

the third band <300 nm is hidden under a marked increase in absorbance, which is probably due to a charge-transfer band involving the heterocyclic pyrazolyl rings.

The spectrum of $[L_2V_2O_2(\mu\text{-}CH_3CO_2)_2]^{2+}$ shows the usual two d–d transitions in the visible region typical for vanadyl complexes with σ-donor ligands.

Electrochemical Study. The cyclic voltammetric results for $[L_2V_2(\mu\text{-O})(\mu\text{-}CH_3CO_2)_2](PF_6)_2$ are displayed in Figure 3. Measurements in acetonitrile containing 0.1 M $[TBA]PF_6$ as supporting electrolyte over the potential range +1.2 to −2.2 V vs ferrocenium/ferrocene (Fc^+/Fc) revealed two reversible one-electron waves at −0.02 and −1.87 V vs Fc^+/Fc (ΔE_p = 70 mV for both processes at a scan rate of 20 mV s^{-1}). Controlled-potential coulometry experiments at potentials +0.5 and −2.1 V vs Fc^+/Fc measured 1.0 ± 0.1 and 1.0 ± 0.2 e mol^{-1} of vanadium(III) dimer. These experiments clearly show that the cation $[L_2V_2(\mu\text{-O})(\mu\text{-}CH_3CO_2)_2]^{2+}$ may be reversibly oxidized by one electron

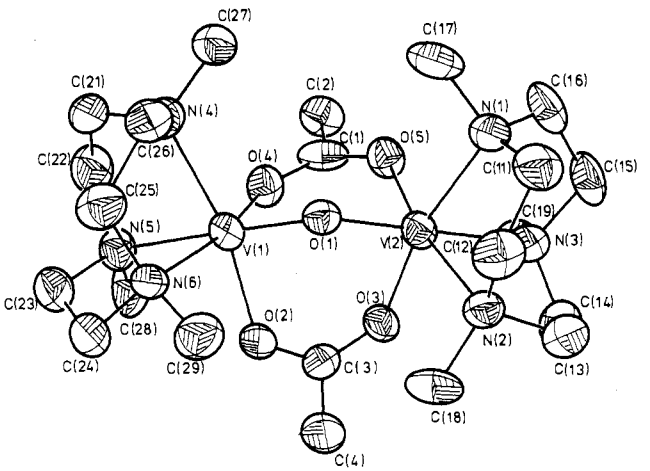

Figure 4. Structure of the cation in $[L_2V_2(\mu\text{-O})(\mu\text{-}CH_3CO_2)_2]I_2\cdot 2H_2O$ showing 40% probability thermal ellipsoids and the atom-labeling scheme.

to produce the mixed-valent $V^{III}V^{IV}$ dimer or it may be reduced by one electron to afford a $V^{III}V^{II}$ mixed-valent dimer:

$$[LV^{III}(\mu\text{-O})(\mu\text{-}CH_3CO_2)_2V^{IV}L]^{3+} \underset{-e^-}{\overset{+e^-}{\rightleftharpoons}} [LV^{III}(\mu\text{-O})(\mu\text{-}CH_3CO_2)_2V^{III}L]^{2+} \underset{-e^-}{\overset{+e^-}{\rightleftharpoons}} [LV^{III}(\mu\text{-O})(\mu\text{-}CH_3CO_2)_2V^{II}L]^{+}$$

The cyclic voltammogram of $[L_2V_2(\mu\text{-O})(\mu\text{-}CH_3CO_2)_2](PF_6)_2$

Table VIII. Comparison of Structural Data for $[L_2M_2(\mu\text{-}O)(\mu\text{-}CH_3CO_2)_2]^{2+}$ Complexes (L = 1,4,7-Trimethyl-1,4,7-triazacyclononane) from Ref 3, 4, and 8

	V	Mn	Fe
$M\text{-}O_{oxo}$, Å	1.792 (4)	1.810 (4)	1.800 (3)
$M\text{-}O_{Ac}$, Å	2.055 (5)	2.047 (4)	2.034 (3)
M–N,[a] Å	2.219 (5), 2.158 (5)	2.232 (5), 2.131 (7)	2.268 (6), 2.198 (4)
M···M, Å	3.250 (2)	3.084 (3)	3.12 (1)
M–O–M, deg	130.2 (2)	120.9 (1)	119.7 (1)

[a] The first value corresponds to the M–N distance trans to the μ-oxo bridge.

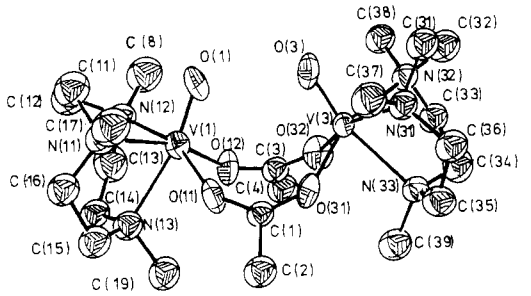

Figure 5. Structure of the cation in $[L_2V_2O_2(\mu\text{-}CH_3CO_2)_2]I_2$ showing 40% probability thermal ellipsoids and the atom-labeling scheme.

measured in aqueous 0.1 M $LiClO_4$ at a glassy-carbon electrode shows in the potential range −1.5 to +1.5 V vs NHE no electrochemical activity.

Crystal Structures. The structure of $[L_2V_2(\mu\text{-}O)(\mu\text{-}CH_3CO_2)_2]I_2\cdot 2H_2O$ consists of the dinuclear cation $[L_2V_2(\mu\text{-}O)(\mu\text{-}CH_3CO_2)_2]^{2+}$, iodide anions, and water of crystallization. Figure 4 shows the atom-labeling scheme and a perspective view of the cation. The vanadium(III) centers are in a distorted-octahedral environment of three amine nitrogen atoms of the macrocycle and three oxygen atoms of one μ-oxo bridge and two symmetrical μ-acetato groups, respectively. The longest V–N bond in the dimer is the one trans to the bridging oxo group (Table III). The structural trans influence of this ligand has also been observed in the analogous iron(III) and manganese(III) complexes.[3,4] The V–O distances are short and comparable to those in the Mn(III) and Fe(III) dimers; they agree well with those reported for $(thf)_3Cl_2V\text{-}O\text{-}VCl_2(thf)_3$ (V–O = 1.769 (5) Å) (thf = tetrahydrofuran), which is a linearly oxo bridged dimer of vanadium(III).[13] The V–O–V angle of 130.2 (2)° is about 10° larger than those found in the iron(III) and manganese(III) analogues, and consequently, the M···M distance in the vanadium(III) dimer is the largest observed in this series of complexes (3.250 (2) Å) (Table VIII). Interestingly, the Shannon ionic radii[14] of high-spin-configured M^{3+} cations in an octahedral ligand field are very similar for V^{3+}, Mn^{3+}, and Fe^{3+} (~0.78 Å). Therefore, it is not clear what factors cause the increase of the M···M distance in the vanadium(III) complex.

The structure of $[L_2V_2O_2(\mu\text{-}CH_3CO_2)_2]I_2$ consists of the dimeric cations $[L_2V_2O_2(\mu\text{-}CH_3CO_2)_2]^{2+}$ and uncoordinated iodide ions. There are two crystallographically independent cations in the unit cell. Within experimental error the dimensions of these two cations are identical (Tables V and VI). Figure 5 shows the atom-labeling scheme and a perspective view of one of the two cations.

The structure of the binuclear vanadyl complex $[L_2V_2O_2(\mu\text{-}CH_3CO_2)_2]^{2+}$ comprises two pseudooctahedral vanadyl(IV) ions bridged by two symmetrical acetate groups. The coordination spheres of the vanadium(IV) atoms are completed by facially coordinating, tridentate, macrocyclic amine ligands and terminal oxo groups. The pseudooctahedral geometry around each vanadium(IV) center appears to be quite normal. The average V–N distance trans to the very short vanadium–oxo bond (average V=O = 1.567 Å) is rather long (2.334 Å) as compared to the V—N distances cis to this oxo group (average 2.170 Å). This indicates the strong trans influence of the vanadyl group.

In the bis(μ-acetato)-bridged dimer the V=O groups adopt syn positions with respect to each other; the two symmetrical acetate groups are the only bridging groups, and the dimeric structure is not supported by additional oxo/hydroxo bridges. The nonbonding distance between the two terminal oxo groups is surprisingly short (2.73 Å) whereas the V···V distance is long (4.075 (2) Å). In contrast, in the binuclear complex $[([9]\text{-}aneN_3)_2V_2O_2(\mu\text{-}OH)_2]Br_2$ the two V=O groups are anti with respect to each other[15] and the V···V distance is 3.033 (3) Å. It is not clear to us why the syn configuration prevails in $[L_2V_2O_2(\mu\text{-}CH_3CO_2)_2]I_2$ over the also possible anti configuration. It is conceivable that this is the favored configuration of the kinetically controlled O_2 oxidation of $[L_2V_2(\mu\text{-}O)(\mu\text{-}CH_3CO_2)_2]^{2+}$, but the synthesis from $LVOCl_2$ and acetate also gives the syn product, which may merely reflect the fact that *syn*-$[L_2V_2O_2(\mu\text{-}CH_3CO_2)_2]I_2$ has a lower solubility than the anti isomer. An anti ⇌ syn equilibrium may exist in solution. It is noted that the geometry of the present bis(μ-acetato)bis(oxovanadium(IV) unit has some resemblance with the cyclic structure $Na_4(VO)(CF_3CO_2)_8(thf)_6(H_2O)_2$ reported recently by Cotton and coworkers,[16] where a VO moiety is bridged by two trifluoroacetato bridges to a sodium cation.

Table IX. Magnetic Properties of $[LM(\mu\text{-}O)(\mu\text{-}CH_3CO_2)_2ML]^{0/2+}$ Complexes ($H = -2J\tilde{S}_1\cdot\tilde{S}_2$)

complex	J, cm^{-1}	coupling	ref
L = 1,4,7-trimethyl-1,4,7-triazacyclononane			
Fe(III) (d^5–d^5, high spin)	−119	antiferromag	21
Mn(III) (d^4–d^4, high spin)	+9	ferromag	22
V(III) (d^2–d^2)	+22	ferromag	this work
L = hydrotripyrazolylborate(1−)			
Fe(III) (d^5–d^5, high spin)	−121	antiferromag	5
Mn(III) (d^4–d^4, high spin)	−0.5	none	6
V(III) (d^2–d^2)	+5	ferromag	this work

Magnetic Properties. Measurements of the molar susceptibility were carried out on solid samples by using the Faraday method between 98 and 298 K. For all binuclear complexes, the temperature-dependent magnetic behavior was modeled by using the theory of Heisenberg, Dirac, and van Vleck for magnetic coupling in a binuclear system. The expressions[17] for the temperature-dependent susceptibility may be derived from the general isotropic exchange Hamiltonian $H = -2J\tilde{S}_1\cdot\tilde{S}_2$, where $S_1 = S_2 = {}^1/_2$ for the vanadium(IV) dimer and $S_1 = S_2 = 1$ for the vanadium(III) dimers, respectively. Since the temperature was varied between 98 and 298 K only, no term was added to correct for paramagnetic impurities and no correction for temperature-independent paramagnetism was carried out.

For $[L_2V_2(\mu\text{-}O)(\mu\text{-}CH_3CO_2)_2]I_2\cdot 2H_2O$ the quantity $\chi_M T$ increases slightly from 2.63 at 293 K to 2.97 to 98 K (or the effective magnetic moment increases with decreasing temperature from 3.25 μ_B per V(III) center at 293 K to 3.44 μ_B per V(III) center at 98 K). Thus, a ferromagnetic spin-exchange coupling is observed. Optimization of the least-squares fit gave $g = 2.1$ (1) and $J = +22$ (1) cm^{-1}. Very similar behavior has been observed for $[L'_2V_2(\mu\text{-}O)(\mu\text{-}CH_3CO_2)_2]$ although the ferromagnetic exchange coupling was found to be much weaker: $g = 2.2$ (1) and $J = +5$ (1) cm^{-1}. $\chi_M T$ increases here from 2.53 at 293 K to 2.84 at 98 K (μ_{eff} = 3.18 μ_B per V(III) (293 K) and 3.36 μ_B (98 K)). To the best of our knowledge these two binuclear complexes represent the first ferromagnetically coupled vanadium(III) dimers.[26] It is of interest to compare these data with those of the antiferromagnetically coupled dimers $Cp_2V_2(\mu\text{-}RCO_2)_4$, where $-J$ varies

(13) Chandrasekhar, P.; Bird, P. H. *Inorg. Chem.* **1984**, *23*, 3677.
(14) Shannon, R. D. *Acta Crystallogr., Sect. A: Cryst. Phys., Diffr., Theor. Gen. Crystallogr.* **1976**, *A32*, 751.
(15) Wieghardt, K.; Bossek, U.; Volckmar, K.; Swiridoff, W.; Weiss, J. *Inorg. Chem.* **1984**, *23*, 1387.
(16) Cotton, F. A.; Lewis, G. E.; Mott, G. N. *Inorg. Chem.* **1983**, *22*, 1825.
(17) O'Connor, C. J. *Prog. Inorg. Chem.* **1979**, *29*, 204.

Chart I

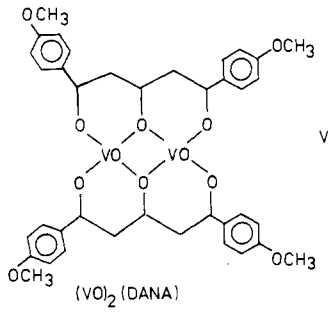

V···V ~ 3.0 - 3.1 Å
J = - 80 cm^{-1}
ref. [20]

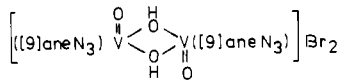

V···V 3.033 Å
J = - 177 cm^{-1}
ref. [15] [23]

between 110 and 165 cm^{-1} depending on R. The V···V distances are between 3.63 and 3.70 Å,[18] which excludes direct metal–metal bonding. In $[Et_4N][V_2Cl_9]$, a complex with three μ-chloro bridges, antiferromagnetic exchange coupling between the two V(III) centers is also observed (J = −40 cm^{-1}).[19]

Interestingly, in $[L_2Mn_2(\mu\text{-}O)(\mu\text{-}CH_3CO_2)_2]^{2+}$ the two manganese(III) centers (d^4–d^4 high spin) are again ferromagnetically coupled, whereas the corresponding iron(III) analogue exhibits strong antiferromagnetic coupling (Table IX). Substitution of the macrocycle 1,4,7-trimethyl-1,4,7-triazacyclononane for hydrotripyrazolylborate(1−) ligands in complexes containing the $[M_2(\mu\text{-}O)(\mu\text{-}CH_3CO_2)_2]^{2+}$ core and a transition metal with a d^n configuration of $n < 5$ apparently decreases the ferromagnetic exchange interaction (Table IX). In contrast, for the vanadyl complex $[L_2V_2O_2(\mu\text{-}CH_3CO_2)_2]I_2$ a strong intramolecular antiferromagnetic spin-exchange coupling is observed. $\chi_M T$ decreases with decreasing temperature; the effective magnetic moment per V(IV) center decreases from 1.60 μ_B at 293 K to 0.85 μ_B at 113 K. An excellent fit of data was found with J = −114 (2) cm^{-1} and g = 2.2 (1). There are two other binuclear vanadyl(IV) complexes in the literature whose magnetic susceptibilities have been measured as a function of temperature. They all exhibit intramolecular antiferromagnetic coupling (Chart I).

From single-crystal EPR measurements on the complex $[([9]aneN_3)_2V_2O_2(\mu\text{-}OH)_2]Br_2$ it has been implied previously[23] that a direct overlap of d_{xy} orbitals that contain the unpaired electron (through space) is the dominant magnetic exchange pathway and not a $d_{x^2-y^2}{}^1$–$d_{x^2-y^2}{}^1$ superexchange interaction via the bridging oxygen atoms. The same mechanism might operate in the present system, although it must be kept in mind that the nonbonding V···V distance in $[L_2V_2O_2(\mu\text{-}CH_3CO_2)_2]I_2$ is 4.075 Å, which could account for the weaker exchange interaction as compared to the bis(μ-hydroxo)-bridged species. Acetate bridges will mediate antiferromagnetic coupling of at most −4 cm^{-1} as a comparison with carboxylate-bridged compounds suggests.[24] If this model is correct, then the weaker interaction in $(VO)_2$(DANA) is not explicable since the V···V distance is approximately the same as in $[([9]aneN_3)_2V_2O_2(\mu\text{-}OH)_2]Br_2$ but J is only −80 cm^{-1}. On the other hand, $(VO)_2$(DANA) is the only species in this series where there is no X-ray structure available; the given V···V distance is an educated estimate.

It is also of considerable interest to compare these results with magnetic measurements on the simple oxovanadium(IV) diacetate, $VO(CH_3CO_2)_2$, the crystal structure of which is also unknown. Here the temperature-dependent magnetic susceptibility was successfully fitted to the Ising model of an infinite linear antiferromagnetic chain with a spin-exchange coupling constant, J, of −166 cm^{-1}. The chain is proposed to contain a V=O···V=O···V moiety with bridging acetate groups.[25]

Acknowledgment. We are grateful to Professor F. A. Cotton for support during the structure determination of $[L_2V_2O_2(\mu\text{-}CH_3CO_2)_2]I_2$ in his laboratory. This work was supported by the Fonds der Chemischen Industrie.

Registry No. $LVCl_3$, 112087-96-4; $LVOCl_2$, 112087-97-5; $[L_2V_2(\mu\text{-}O)(\mu\text{-}CH_3CO_2)_2]I_2{\cdot}2H_2O$, 106264-13-5; $[L'_2V_2(\mu\text{-}O)(\mu\text{-}CH_3CO_2)_2]$, 112112-46-6; $[L_2V_2O_2(\mu\text{-}CH_3CO_2)_2]I_2$, 112087-98-6; $[L_2V_2(\mu\text{-}O)(\mu\text{-}CH_3CO_2)_2](PF_6)_2$, 112088-00-3; $[LV^{III}(\mu\text{-}O)(\mu\text{-}CH_3CO_2)_2V^{IV}L]^{3+}$, 112088-01-4; $[LV^{III}(\mu\text{-}O)(\mu\text{-}CH_3CO_2)_2V^{II}L]^{+}$, 112088-02-5.

Supplementary Material Available: Tables S1–S4, listing anisotropic thermal parameters, calculated positions of hydrogen atoms, bond distances, and bond angles for $[L_2V_2(\mu\text{-}O)(\mu\text{-}CH_3CO_2)_2]I_2{\cdot}2H_2O$ and Tables S6–S8, listing anisotropic thermal parameters, bond distances, and bond angles, for $[L_2V_2O_2(\mu\text{-}CH_3CO_2)_2]I_2$ (12 pages); Tables S5 and S9, listing calculated and observed structure factors for the two compounds (41 pages). Ordering information is given on any current masthead page.

(18) (a) Larin, G. M.; Kalinnikov, V. T.; Aleksandrov, G. G.; Struchkov, Yu. T.; Pasynskii, A. A.; Kolobova, N. E. *J. Organomet. Chem.* **1971**, *27*, 53. (b) Kirillova, N. I.; Gusev, A. I.; Pasynskii, A. A.; Struchkov, Yu. T. *Zh. Strukt. Khim.* **1972**, *13*, 880. (c) Kalinnikov, V. T.; Zelentsov, V. V.; Larin, G. M.; Pasynskii, A. A.; Ubozhenko, D. D. *Zh. Obshch. Khim.* **1972**, *42*, 2692.
(19) Hodgson, D. J. *Prog. Inorg. Chem.* **1975**, *19*, 173.
(20) Heeg, M. J.; Mack, J. L.; Glick, M. D.; Lintvedt, R. L. *Inorg. Chem.* **1981**, *20*, 833.
(21) Hartman, J. R.; Rardin, R. L.; Chaudhuri, P.; Pohl, K.; Wieghardt, K.; Nuber, B.; Weiss, J.; Papaefthymiou, G. C.; Frankel, R. B.; Lippard, S. J. *J. Am. Chem. Soc.* **1987**, *109*, 7387.
(22) Girerd, J. J.; Wieghardt, K., unpublished results.
(23) Ozarowski, A.; Reinen, D. *Inorg. Chem.* **1986**, *25*, 1704.
(24) (a) Cheng, C.; Reiff, W. M. *Inorg. Chem.* **1977**, *16*, 2097. (b) Reem, R. C.; Solomon, E. I. *J. Am. Chem. Soc.* **1987**, *109*, 1216. (c) Pierce, R. D.; Friedberg, S. A. *Phys. Rev. B: Solid State* **1971**, *3*, 934.
(25) (a) Casey, A. T.; Thackeray, J. R. *Aust. J. Chem.* **1969**, *22*, 2549. (b) Casey, A. T.; Morris, B. S.; Sinn, E.; Thackeray, J. R. *Aust. J. Chem.* **1972**, *25*, 1196. (c) Dakternieks, D. R.; Harris, C. M.; Milham, P. J.; Morris, B. S.; Sinn, E. *J. Inorg. Nucl. Chem.* **1969**, *5*, 97. (d) Walter, J. P.; Dartiguenave, M.; Dartiguenave, Y. *J. Inorg. Nucl. Chem.* **1973**, *35*, 3207.
(26) As a reviewer has pointed out, the largest deviation from the spin-only magnetic moment can in principle be caused by the orbital contribution, which may be temperature-dependent.